

## Crystallographic Aspects Regarding the Insertion of Ag<sup>+</sup> Ions into a Hydroxyapatite Structure

Ivory Marcos Gomes dos Santos<sup>a</sup>, Larissa Souza Noel Simas Barbosa<sup>b</sup>, Cristiane Xavier Resende<sup>a</sup>,  
Glória de Almeida Soares<sup>b</sup>, Euler Araujo dos Santos<sup>a\*</sup>

<sup>a</sup>Laboratório de Biomateriais, Programa de Pós-Graduação em Ciência e Engenharia de Materiais, Universidade Federal de Sergipe – UFS, Av. Marechal Rondon, s/n, CEP 49100-000, São Cristóvão, SE, Brazil

<sup>b</sup>Departamento de Engenharia Metalúrgica e de Materiais, Instituto Alberto Luiz Coimbra de Pós-Graduação e Pesquisa de Engenharia – COPPE, Universidade Federal do Rio de Janeiro – UFRJ, CP 68505, CEP 21941-972, Rio de Janeiro, RJ, Brazil

Received: August 5, 2015; Revised: August 19, 2015

The objective of this study was to evaluate how silver can be inserted into hydroxyapatite (HA) via two distinct processes: co-doping with CO<sub>3</sub><sup>2-</sup> via precipitation in an aqueous medium and immersion of preformed HA crystals into Ag<sup>+</sup> solutions. It was concluded that although Ag<sup>+</sup> and Ca<sup>2+</sup> have different radii, the accommodation of Ag<sup>+</sup> ions in the Ca<sup>2+</sup> sites of the hydroxyapatite lattice can be explained by the models proposed for inserting monovalent ions such as Na<sup>+</sup>. In this case, because Ag<sup>+</sup> ions are larger than Ca<sup>2+</sup> ions and have a different charge, the Ag<sup>+</sup> ions are stabilized in the HA structure by co-substitution with CO<sub>3</sub><sup>2-</sup> ions in both the A- and B-type sites. This simultaneous insertion of Ag<sup>+</sup> and CO<sub>3</sub><sup>2-</sup> appears to thermally stabilize the HA phase because no phase transformation is observed after calcination. In addition, the doping of HA with Ag<sup>+</sup> ions can clearly occur via two routes: co-precipitation in the presence of these ions or diffusion in preformed hydroxyapatite crystals. This result appears to indicate the possibility of doping HA with Ag<sup>+</sup> using less complex routes at ambient temperature and with prefabricated implants or biomaterials, which reduces the costs of producing devices with antibacterial effects.

**Keywords:** *hydroxyapatite, silver, doping, carbonate, diffusion*

### 1. Introduction

In general, pathogenic bacteria survive in colonies called biofilms, which provide protection against antibiotic agents and ensure proliferation of the bacteria. The bacteria in the innermost biofilm tend to receive a lower dosage of antibiotic than those at the biofilm surface, which generates favorable conditions for developing resistance against antibiotics.

Antibiotics have systemic action, are not localized, and can affect all bacteria living in the body, even the non-pathogenic bacteria that have fundamental roles in physiology. Thus, the development of new techniques to combat bacteria has been focused on formulating drugs that can be precisely vectorized to the affected area<sup>1</sup>. The association of these drugs with implantable devices through either adsorption or absorption has frequently been considered a method for vectorizing antibiotics to affected areas<sup>2</sup>.

The use of silver as an antibiotic agent is currently experiencing a resurgence in medicine. Silver has been known to possess antibiotic activity since ancient times, and it is a viable alternative to common antibiotics because it has a broad spectrum of activity toward different types of bacteria<sup>3</sup>. The use of silver, even in small quantities<sup>4</sup>, provides a strong antibiotic effect that accelerates the efficacy of treatments. The use of silver is economically feasible compared to the costs for producing a new antibiotic or for modifying an

existing one. Problems related to chemical and thermal stability, denaturation, and storage conditions make common antibiotics considerably more complex in terms of synthesis and handling than silver and its compounds. Consequently, several attempts have been made to associate silver and its compounds with biomaterials and implantable devices<sup>4-6</sup>.

Implantable devices composed of hydroxyapatite (HA), particularly those used in ostomies, are constantly exposed to bacteria, which can use these devices as body-invasion gateways. Thus, HA doped with silver or containing silver nanoparticles has been proposed as a method to reduce or avoid such contamination. However, the introduction of silver into an apatite structure can generate crystalline defects, which can lead to substantial thermal instability. In most cases, after thermal treatments of doped HA at high temperatures, phase transformations and the formation of less biocompatible phosphates and even calcium oxide, which are toxic to cells, occur.

Sygnatowicz et al.<sup>7</sup> observed a phase transformation in an HA that contained 5-10 wt% Ag<sup>+</sup>, along with the formation of β-tricalcium phosphate (β-TCP), after calcination at 800 °C and 900 °C. Other studies also demonstrated the formation of this phase for various Ag<sup>+</sup> concentrations<sup>8,9</sup>. In most cases, the decrease in Ag<sup>+</sup> concentration corresponds to a smaller phase transformation.

\*e-mail: [euler.ufs@gmail.com](mailto:euler.ufs@gmail.com)

Recent reports in the literature indicate the possibility of achieving a thermally stable HA using a co-doping process, where ions with different sizes and charges are inserted into the apatite lattice. Silva et al.<sup>10</sup> demonstrated that Sr-containing HA could be thermally stabilized by simultaneously inserting Na<sup>+</sup>, Cl<sup>-</sup> and CO<sub>3</sub><sup>2-</sup> into the apatite lattice. Similarly, Moreira et al.<sup>11,12</sup> demonstrated that simultaneously adding Mg<sup>2+</sup>, Mn<sup>2+</sup> and Sr<sup>2+</sup> ions into the apatite lattice stabilized the crystal and prevented phase transformations after calcination at 1000 °C. Aina et al.<sup>13</sup> showed that Mg<sup>2+</sup>- or Sr<sup>2+</sup>-doped apatites exhibited a phase transformation after thermal treatment, whereas the samples that contained both Mg<sup>2+</sup> and Sr<sup>2+</sup> did not.

Kumar et al.<sup>14</sup> observed that inserting both Zn<sup>2+</sup> and CO<sub>3</sub><sup>2-</sup> into the apatite structure diminished the formation of TCP phases after calcination at 1300 °C compared to the insertion of only Zn<sup>2+</sup>. The vacancies generated by the replacement of PO<sub>4</sub><sup>3-</sup> groups with CO<sub>3</sub><sup>2-</sup> (different charges) were compensated by the replacement of Ca<sup>2+</sup> with Zn<sup>2+</sup> (different sizes). Similarly, Mostafa et al.<sup>15</sup> investigated the co-doping of HA with Na<sup>+</sup>, CO<sub>3</sub><sup>2-</sup> and SiO<sub>4</sub><sup>4-</sup>. They demonstrated that the simultaneous introduction of Na<sup>+</sup> and CO<sub>3</sub><sup>2-</sup> could stabilize the structure, thereby preventing phase transformations, even at 1100 °C.

These studies demonstrated that inserting ions of different sizes and charges into HA could compensate for the structural stress caused by inserting a single type of ion. Thus, a method to insert ions that present stability problems into the HA structure, such as silver, is the co-doping process.

Accordingly, understanding how Ag<sup>+</sup> ions can be stabilized in the HA lattice is essential for proposing appropriate mechanisms to manufacture implantable devices that are resistant to bacteria without reducing the biocompatibility caused by possible phase transformations. Thus, the objective of this study is to understand how Ag<sup>+</sup> ions can be introduced into the HA structure using two methods: HA co-precipitation in the presence of Ag<sup>+</sup> and CO<sub>3</sub><sup>2-</sup> and diffusion of Ag<sup>+</sup> ions into preformed HA crystals.

## 2. Materials and Methods

### 2.1. Hydroxyapatite synthesis

Hydroxyapatite (HA) was synthesized using the precipitation method in an aqueous medium through a typical acid-base reaction between calcium hydroxide [Ca(OH)<sub>2</sub>] and phosphoric acid [H<sub>3</sub>PO<sub>4</sub>] at concentrations of 0.198 and 0.119 mol/L, respectively. The acid solution was added dropwise (2.0 mL/min) to the basic solution under constant agitation. The pH value was monitored and maintained at 10 or greater during the reaction. The synthesis of the control was performed using potassium hydroxide (KOH). The temperature was maintained at 37 °C throughout the entire synthesis. The obtained suspension was aged under the same temperature and pH conditions for 24 hours. Subsequently, the suspension was filtered and washed with distilled water until the supernatant was neutral (pH ≈ 7). The precipitate was dried at 120 °C for 24 hours.

The Ag<sup>+</sup>-doped HA was synthesized following an identical procedure. However, silver nitrate (AgNO<sub>3</sub>) was added to phosphoric acid to obtain a final Ag<sup>+</sup> concentration

of  $2.5 \times 10^{-4}$  mol/L. In both cases, the atmosphere was not controlled to allow free insertion of CO<sub>3</sub><sup>2-</sup> into the HA structure.

The obtained HA powders were calcined at 1000 °C for 2 hours with a heating rate of 2.8 °C/min to determine their thermal stability at high temperature.

### 2.2. Ag<sup>+</sup> diffusion in hydroxyapatite crystals

A suspension of pure HA (without Ag<sup>+</sup>) was prepared using a 0.1 mol/L silver nitrate solution. This suspension was constantly stirred at 23 °C for 1, 24, 48 and 70 hours. After each time period, the suspension was filtered and washed with distilled water to remove soluble ions. The obtained powder was dried at 120 °C for 24 hours.

### 2.3. Composition

The synthesized samples were analyzed using wavelength-dispersive X-ray fluorescence (WDXRF) to identify the present elements and their quantity. The powders were pressed without adding boric acid to create pellets, which were analyzed directly using a WDXRF spectrometer (Bruker, Tiger S8).

The CO<sub>3</sub><sup>2-</sup>, PO<sub>4</sub><sup>3-</sup> and OH<sup>-</sup> groups were observed using Fourier transform infrared spectroscopy (FTIR). The changes in these groups were followed by calculating the relative area under the curves (deconvolution). All the curves were normalized by the intensity of the vibrational mode  $\nu_4$  PO<sub>4</sub> at 572 cm<sup>-1</sup>. The analyses were conducted in absorbance mode from 4000 to 400 cm<sup>-1</sup> (step size of 4 cm<sup>-1</sup>) using a Perkin-Elmer (Spectrum BX) spectrometer.

### 2.4. Crystalline structure

The samples were characterized before and after calcination using X-ray diffraction (XRD) to identify the crystalline phases and possible structural and morphological changes induced by the Ag<sup>+</sup> doping. The XRD patterns were obtained under the following conditions:  $\theta/2\theta$  of 5-60°, continuous scan (2°/min), step size of 0.02° and radiation generated at 40 kV/40 mA ( $\lambda_{\text{CoK}\alpha} = 1.7902 \text{ \AA}$ ). The analyses were performed using a RIGAKU DMAX 100 diffractometer.

#### 2.4.1. Lattice parameters

The *a* and *c* lattice parameters and cell unit volume were calculated using the Rietveld method for structure refinement and a convolution-based approach for the profile fitting, which was implemented using X'Pert HighScore Plus software. CIF files corresponding to the JCPDS cards HA: 9-432;  $\alpha$ -TCP: 29-0359;  $\beta$ -TCP: 9-169; Ag<sub>3</sub>(PO<sub>4</sub>)<sub>4</sub>: 6-505; Ag<sub>2</sub>: 4-783; CaO: 37-1497, were used in the structure refinement.

#### 2.4.2. Crystallite size and asymmetry

The crystallite size (*L*) was estimated using the Scherrer equation<sup>16</sup> considering the (*h k l*) plane of HA according to the following equation:

$$L = \frac{0.89\lambda}{B_{hkl} \cos \theta} \quad (1)$$

where  $\lambda$  is the incident radiation wavelength (nm);  $B_{hkl}$  is the full width at half maximum (FWHM), which was corrected by subtracting from that measured using the main

diffraction peak of LaB<sub>6</sub> (under identical conditions); and  $\theta$  is the diffraction angle that corresponds to the (0 0 2) plane for K $\alpha$ Co.

The asymmetry of the crystal was determined from the relation between the peak intensities that corresponded to the (2 0 0) and (0 0 3) planes, *i.e.*, the [1 0 0] and [1 0 0] directions, respectively.

### 2.4.3. Crystal morphology after immersion in Ag<sup>+</sup> solution

The HA powder after immersion in the Ag<sup>+</sup> solution was analyzed using transmission electron microscopy (TEM) in a JEOL 2000FX microscope operated at 200 kV to evaluate possible changes in the crystal morphology of HA.

## 3. Results and Discussion

### 3.1. Doping by co-precipitation

#### 3.1.1. Vacancy formation

Quantitative analyses using wavelength-dispersive X-ray fluorescence (WDXRF) enabled us to determine the quantities of Ag, Ca and P in the samples (Table 1). The obtained Ca/P ratio in the HA sample was consistent with the expected value for a stoichiometric hydroxyapatite (1.67). However, the inclusion of Ag<sup>+</sup> (HA-Ag) slightly increased the value of (Ag+Ca)/P to 1.69. If we consider that Ag<sup>+</sup> ions can only occupy the positive Ca<sup>2+</sup> sites, the necessary charge balance to maintain the neutrality of the HA structure is compromised. In this case, the entry of other ions with different charges may be facilitated during crystal growth to restore neutrality.

**Table 1.** Relative quantities of the elements in the samples, which were measured using WDXRF.

Sample	Composition (mol %)			(Ca+Ag/P)
	Ca	P	Ag	
HA	13.81	8.27	-	1.67
HA-Ag	14.54	8.61	0.1	1.69

It is known that the inclusion of monovalent ions such as Na<sup>+</sup> can generate favorable conditions to accommodate CO<sub>3</sub><sup>2-</sup> in PO<sub>4</sub><sup>3-</sup> sites<sup>17</sup>. This accommodation restores the neutrality of the solid and can also explain the increase in the (Ag+Ca)/P ratio because the quantity of PO<sub>4</sub><sup>3-</sup> in the structure is reduced.

Because the synthesis atmosphere was not controlled in our experiments, CO<sub>2</sub> from the air was free to be inserted into the HA structure as CO<sub>3</sub><sup>2-</sup>. Indeed, the precipitation method for producing HA in aqueous media tends to promote the dissolution of CO<sub>2</sub> and the consequent insertion of CO<sub>3</sub><sup>2-</sup> into the HA structure<sup>18-20</sup> when it is performed under alkaline conditions at low temperatures.

Vignoles<sup>21</sup> proposed a model to describe the structure of a hydroxyapatite containing Na<sup>+</sup> and CO<sub>3</sub><sup>2-</sup>:



where  $0 \leq x \leq 3$

In this model, the insertion of a monovalent ion such as Na<sup>+</sup> in the Ca<sup>2+</sup> sites simultaneously generates the conditions for inserting CO<sub>3</sub><sup>2-</sup> ions and produces vacancies in the pairs (Na<sup>+</sup>/OH<sup>-</sup>). There are reports in the literature that demonstrate that the OH<sup>-</sup> infrared absorption bands decrease when the Na<sup>+</sup> concentration increases in HA structures<sup>22-24</sup>.

Fourier transform infrared spectroscopy (FTIR) analyses allowed us to verify the typical HA groups in all samples. A zoom scan in the region of 660-540 cm<sup>-1</sup> revealed details from the OH<sup>-</sup> and PO<sub>4</sub><sup>3-</sup> group vibrations (Figures 1 and 2). Prior to calcination, the insertion of Ag<sup>+</sup> caused the intensity of the OH<sup>-</sup> bands to decrease (Figure 1). The relative area under the FTIR curves  $\nu_{\text{L}}\text{OH}/\nu_4\text{PO}_4$  calculated from HA and HA-Ag were 0.59 and 0.52, respectively. After calcination, there was no significant difference between the intensities of the OH<sup>-</sup> and PO<sub>4</sub><sup>3-</sup> bands (Figure 2). The relative area under the curves  $\nu_{\text{L}}\text{OH}/\nu_4\text{PO}_4$  calculated from HA and HA-Ag were 0.96 and 0.97, respectively. Therefore, one can assume that the intensities of the OH<sup>-</sup> bands of HA-Ag samples decrease prior to calcination because OH<sup>-</sup> vacancies are generated. Accordingly, the Vignoles model that describes the structure

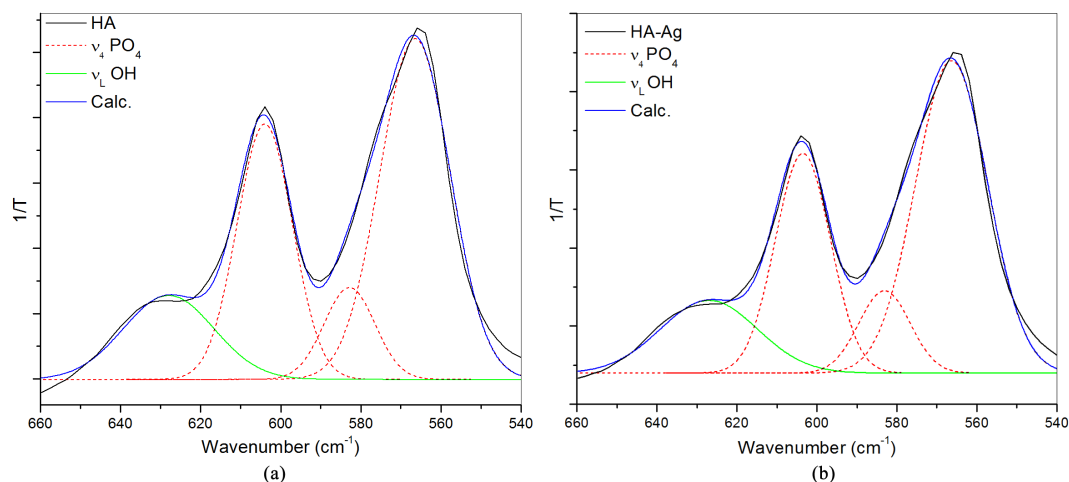
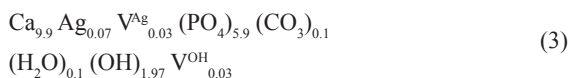


**Figure 1.** Zoom scanning of the FTIR spectra for the vibration regions related to the OH<sup>-</sup> and PO<sub>4</sub><sup>3-</sup> groups, which were obtained from the HA (a) and HA-Ag (b) samples prior to calcination.

of a  $\text{Na}^+$ -doped HA is also suitable for explaining the occupation of the  $\text{Ca}^{2+}$  sites by  $\text{Ag}^+$  ions in HA structures. Thus, assuming this model and considering the molar amount of  $\text{Ag}^+$  measured with WDXRF in our experiment, we obtain the following chemical formula:



### 3.1.2. Occupation of A and B sites for $\text{CO}_3^{2-}$

If we observe in detail the region of  $\text{CO}_3^{2-}$  absorption groups ( $\nu_2$  C-O), there is an adjustment problem with the last model (vacancy formation). The bands in the region of  $871\text{--}880\text{ cm}^{-1}$  confirmed the insertion of  $\text{CO}_3^{2-}$  at both the B-type sites ( $\text{PO}_4^{3-}$ ) and at the A-type sites ( $\text{OH}^-$ ) for the HA-Ag samples prior to calcination (Figure 3). The absorption

bands were distributed between the two regions, indicating the presence of  $\text{CO}_3^{2-}$  at both sites. In fact, the relative area under the FTIR curves calculated from HA and HA-Ag ( $\nu_2\text{CO}_3\text{-A}/\nu_2\text{CO}_3\text{-B}$  ratio) were 0.423 and 0.425, respectively.

After calcination, these bands disappeared from the spectra, which suggests that the heat treatment can remove the majority of  $\text{CO}_3^{2-}$  groups from the HA structure (Figure 4).

Fleet & Liu<sup>23</sup> proposed a model to describe HA doped with monovalent cations such as  $\text{Na}^+$ , which considers the occupation of B- and A-type sites by  $\text{CO}_3^{2-}$  groups at the same time:



Using the quantities of  $\text{Ag}^+$ ,  $\text{Ca}^{2+}$  and  $\text{PO}_4^{3-}$  that were calculated in our work using WDXRF, and assuming the  $\nu_2\text{CO}_3\text{-A}/\nu_2\text{CO}_3\text{-B}$  ratio obtained from FTIR curves we propose the following chemical formula:

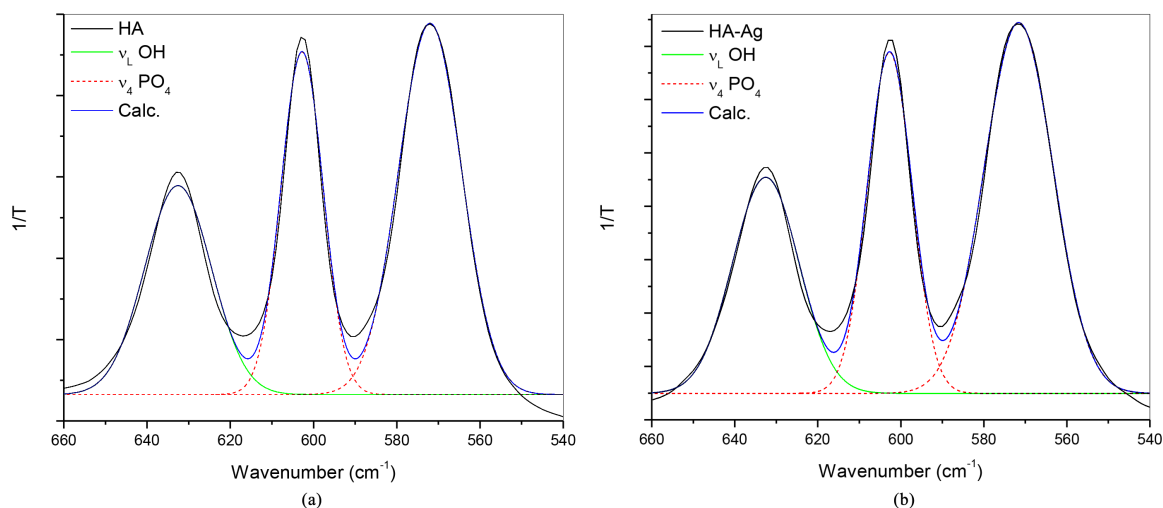


**Figure 2.** Zoom scanning of the FTIR spectra for the vibration regions related to the  $\text{OH}^-$  and  $\text{PO}_4^{3-}$  groups, which were obtained from the HA (a) and HA-Ag (b) samples after calcination at  $1000\text{ }^\circ\text{C}/2\text{ h}$ .

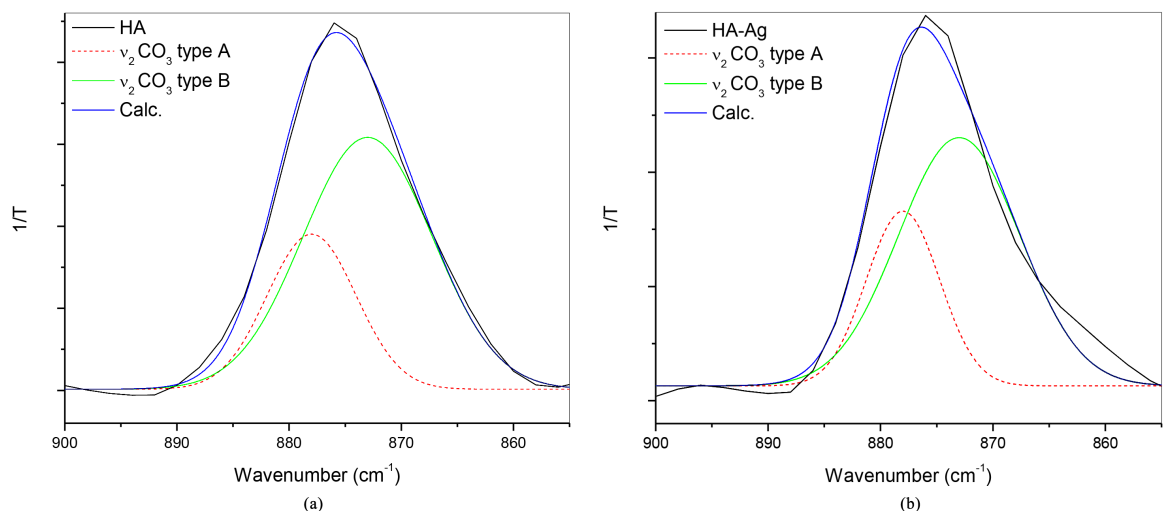


**Figure 3.** Zoom scanning of the FTIR spectra for the vibration regions related to the  $\text{CO}_3^{2-}$  groups, which were obtained from the HA (a) and HA-Ag (b) samples prior to calcination.



In both aforementioned models<sup>21,23</sup>, the Ag/(Ag+Ca) ratio indicates that approximately 0.7% of the Ca<sup>2+</sup> ions were replaced by Ag<sup>+</sup> ions. The (Ag+Ca)/P ratio is 1.69, as calculated using WDXRF. However, this latest model does not consider the formation of vacancies in Na<sup>+</sup>/OH<sup>-</sup> pairs that can justify the reduction in the OH<sup>-</sup> infrared absorption bands, which was observed in our HA-Ag sample prior to calcination (Figure 1). Nevertheless, in this latest model, the reduction in OH<sup>-</sup> groups is equivalent to the amount of monovalent

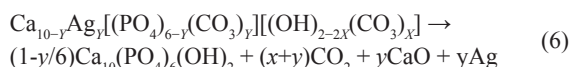
cations that were added into the HA structure. Therefore, the observed reduction in the OH<sup>-</sup> infrared absorption bands in the HA-Ag sample can be adequately explained by the replacement of these groups by CO<sub>3</sub><sup>2-</sup> groups.

In addition, a question arises: why did the intensity of the OH<sup>-</sup> infrared absorption bands of the samples not decrease after calcination?

### 3.1.3. CO<sub>3</sub><sup>2-</sup> release

To answer the last question, it is necessary to recall that the release of CO<sub>3</sub><sup>2-</sup> groups from the structure of a carbonated HA generates CaO as a byproduct<sup>20</sup>. When the CO<sub>3</sub><sup>2-</sup> groups replace the PO<sub>4</sub><sup>3-</sup> groups, the excess Ca<sup>2+</sup> ions tend to react with oxygen to form CaO at temperatures above 600°C.

The release of CO<sub>3</sub><sup>2-</sup> from an A- and B-type carbonated HA, such as that obtained in our work, can be described according the following reaction:



After CO<sub>3</sub><sup>2-</sup> is released from the HA structure, the excess Ca<sup>2+</sup> tends to form CaO, the inserted silver tends to form metallic silver<sup>8,25</sup>, and the remainder generates a stoichiometric hydroxyapatite. Thus, after calcination, the vibrational modes from OH<sup>-</sup> groups may be remarkably enhanced because of the better lattice organization and release of CO<sub>3</sub><sup>2-</sup> from the structure. Indeed, the main peak that corresponds to the (2 0 0) plane of CaO (*d* = 0.2405 nm) (ICDD 37-1497) is not observed in the X-ray diffraction pattern of HA (Figure 5), but it is found in HA-Ag after calcination (Figure 6). The Rietveld results indicated the presence of 0.9 wt.% of CaO. However, the presence of metallic silver could not be

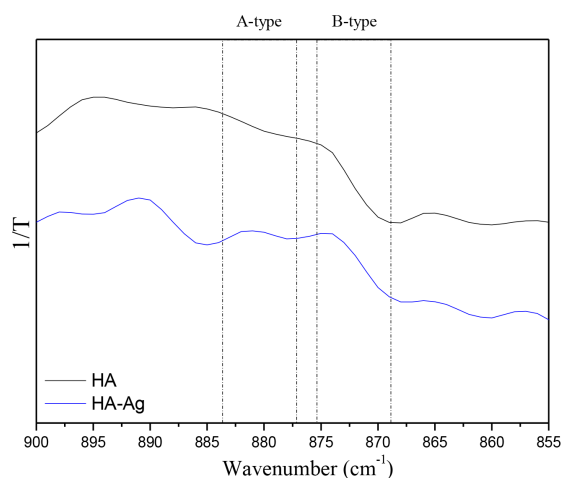


**Figure 4.** Zoom scanning of the FTIR spectra for the vibration regions related to the CO<sub>3</sub><sup>2-</sup> groups, which were obtained from the HA and HA-Ag samples after calcination.

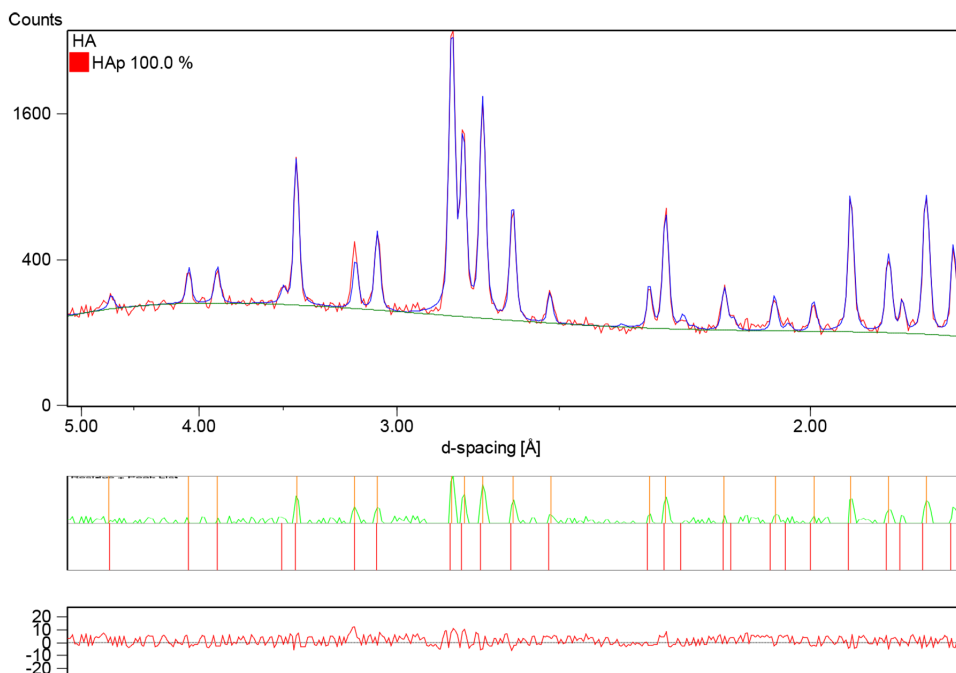
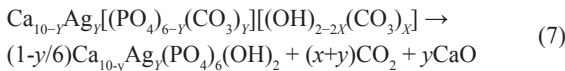


**Figure 5.** X-ray diffraction pattern of the HA sample after calcination at 1000 °C/2 h. Only the hydroxyapatite phase (HAp) was identified by Rietveld refinement. The residue generated from the refinement is show in the graphic (bottom).

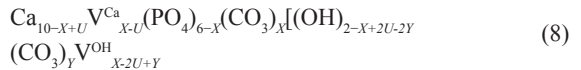
determined because the main peak that corresponds to its (1 1 1) plane was absent ( $d = 0.2359$  nm) (ICDD 4-0783). One can assume that the low quantity of  $\text{Ag}^+$  did not enable the generation of a significant amount of metallic silver to be detected in the experimental conditions of this work. This result can also indicate that  $\text{Ag}^+$  ions were confined in the HA structure even after calcination.

To support this latest hypothesis, it is necessary to assume another  $\text{CO}_3^{2-}$  release model that can consider the formation of only Ag-doped hydroxyapatite and CaO. Thus, we can rewrite the decarbonation reaction as follows:



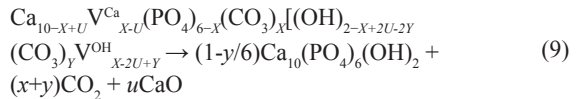
If this model is correct,  $\text{Ag}^+$  ions that are inserted into the HA structure should change the lattice parameters of HA because  $\text{Ag}^+$  ions (0.128 nm) have a different size and charge from  $\text{Ca}^{2+}$  ions (0.099 nm) for identical coordination numbers.

The XRD analyses indicated that HA was formed in all samples (Figures 5 and 6). The three most intense peaks in the diffractograms correspond to the (2 1 1), (1 1 2) and (3 0 0) planes, which are typical for HA. For the pure HA, no phase transformation was observed after calcination. If one considers the FTIR results of the HA prior to calcination, in which the presence of A- and B-type carbonated HA are observed in similar quantities, the only method to produce a stoichiometric HA after calcination is the generation of  $\text{Ca}^{2+}$  vacancies in identical proportions to the  $\text{PO}_4^{3-}$  that is replaced by  $\text{CO}_3^{2-}$ , which will maintain the HA stoichiometry ( $\text{Ca}/\text{P} = 1.67$ ) even after the release of  $\text{CO}_3^{2-}$  from the structure. Therefore, the model proposed by Vignoles<sup>21</sup> can be used to describe this behavior:



where ( $0 < x < 2$ ), ( $0 < 2u < x$ ) and ( $0 < y < 2-x+2u$ )

In this case, to have the quantity of  $\text{Ca}^{2+}$  vacancies notably close to the amount of  $\text{PO}_4^{3-}$  replaced by  $\text{CO}_3^{2-}$ , the value of  $u$  must tend to zero. Therefore, the release of  $\text{CO}_3^{2-}$  is described as follows:



This mechanism can properly explain the observations from both the FTIR and XRD analyses. In fact, the obtained lattice parameters of HA after calcination were similar to those observed for a standard hydroxyapatite (Table 2). In addition, the lattice parameters of HA-Ag exhibited a slight increase in the  $a$  and  $c$  axes relative to the pure HA.

### 3.1.4. Structural changes

Rameshbabu et al.<sup>5</sup> and Badrouir et al.<sup>6</sup> reported that the insertion of  $\text{Ag}^+$  into the HA structure occurred preferentially at the Ca I site, which is the only site in which  $\text{Ca}^{2+}$  ions are

**Table 2.** Comparison between the lattice parameters calculated by Rietveld refinement for the synthesized samples after calcination at 1000 °C/2 h.

Sample	Lattice parameters			
	$a$	$b$	$c$	$V(\text{\AA}^3)$
HA	9.4070	9.4070	6.8722	526.64
HA-Ag	9.4072	9.4072	6.8730	526.70

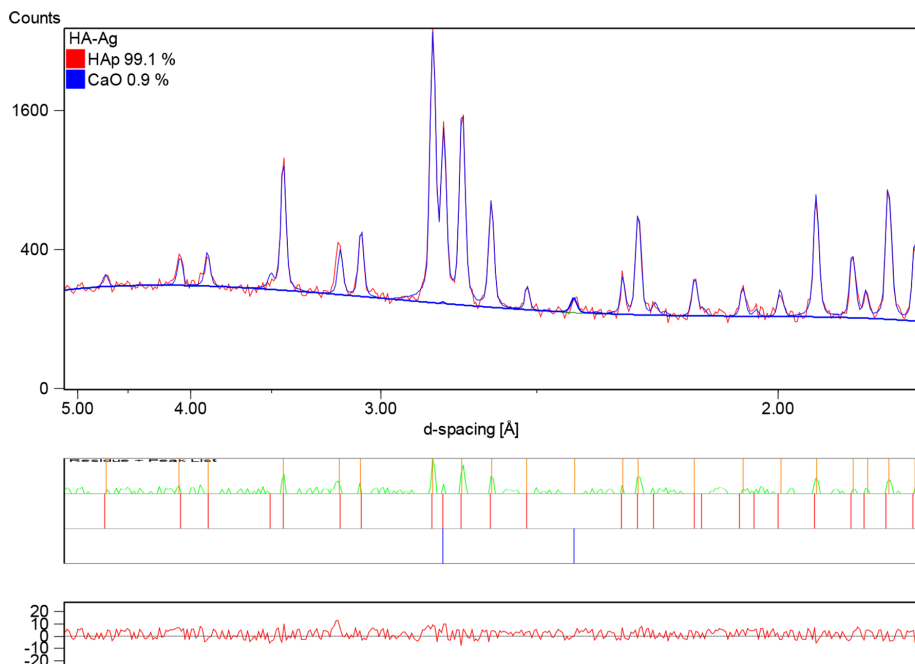


**Figure 6.** X-ray diffraction pattern of the HA-Ag sample after calcination at 1000 °C/2 h. The phases hydroxyapatite (HAp) and calcium oxide (CaO) were identified and quantified by Rietveld refinement. The residue generated from the refinement is shown in the graphic (bottom).

confined among the rigid PO<sub>4</sub><sup>3-</sup> tetrahedral groups. In contrast, according to Singh et al.<sup>9</sup>, Ag<sup>+</sup> ions tend to be incorporated more easily into Ca II sites. In this case, the insertion of Ag<sup>+</sup> is favored by the mobility of the bond between Ca<sup>2+</sup> and hydroxyl groups in the HA channels. The accommodation of Ag<sup>+</sup> ions in the Ca II sites causes the unit cell to expand, which is directly related to the increase in the *a* and *c* lattice parameters. If we consider that the CO<sub>3</sub><sup>2-</sup> ions are completely eliminated after calcination (as suggested by the FTIR data), the increase in the *a* and *c* lattice parameters observed is directly associated with the insertion of Ag<sup>+</sup> ions into the HA lattice. The slight change in the *a* and *c* observed in this work could be explained by the small quantity of Ag<sup>+</sup> replacing Ca<sup>2+</sup>. In fact, less than one Ca<sup>2+</sup> was replaced by Ag<sup>+</sup> ions in a unit cell.

The Rietveld analysis of the respective diffraction pattern included the refinement of the occupancy parameters for the Ca sites, which could be occupied by Ca and Ag atoms under the stoichiometric constraints in the HA phase. The result of the refinement confirmed the Ag atoms in the HA phase, as the replacement of Ca by Ag in the HA phase indeed improved the goodness of fit indices.

The presence of Ag<sup>+</sup> ions in the HA structure slightly decreases the crystallite size of the samples prior to calcination (Figure 7). After calcination, the crystals grow in a similar method, regardless of the presence of Ag<sup>+</sup> ions. The asymmetric nature of these crystals, *i.e.*, their tendency to grow in a preferential direction, was measured. Prior to calcination, the pure HA exhibited more elongated crystals than the HA-Ag samples, which suggests that the insertion of CO<sub>3</sub><sup>2-</sup> ions induces a preferential crystal growth in the *c* direction (Figure 8). Simultaneously, the insertion of Ag<sup>+</sup> ions reduced this growth in the *c* direction and generated conditions to produce more spherical crystals. It is known that the insertion of CO<sub>3</sub><sup>2-</sup> into the B-type sites of HA can decrease the (*h k l*) distances and increase the (*0 0 l*) distances. The opposite behavior is observed when CO<sub>3</sub><sup>2-</sup> ions are placed in the A-type sites<sup>20,26,27</sup>. However, these distortions are much more remarkable when CO<sub>3</sub><sup>2-</sup> is confined in the hydroxyl channels of HA, which may explain the behavior observed in this work.

According to Hwang et al.<sup>27</sup>, the limit distance of Ag<sup>+</sup> diffusion is notably short in HA, which can induce its presence only on the crystal surface depending on the type of synthesis. In our case, the Ag<sup>+</sup> ions were present in the solution during the entire synthesis, which leads us to conclude that this ion is not confined on the surface. Furthermore, if the Ag<sup>+</sup> ions were confined only on the crystal surfaces, the crystal asymmetry might be significantly changed, which was not detected here.

### 3.2. Doping by ion-exchange

To evaluate the diffusion of Ag<sup>+</sup> ions in previously formed HA crystals, we immersed a pure HA into a solution containing Ag<sup>+</sup>. The obtained transmission electron microscopy images allowed us to confirm the presence of nano electro-dense clusters on the HA crystal surface, which may be related to a Ag<sup>+</sup>-rich phase (Figure 9). After 1 hour of immersion, elongated HA crystals was observed without many electro-dense agglomerates. After 24 hours, the amount of agglomerates

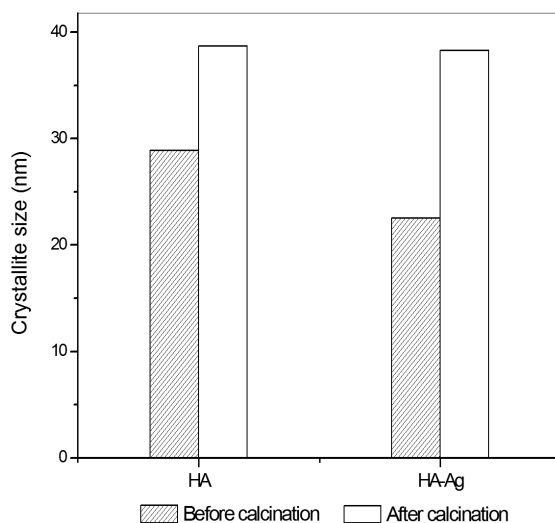


**Figure 7.** Crystallite size calculated from the X-ray diffraction patterns of the samples before and after calcination.

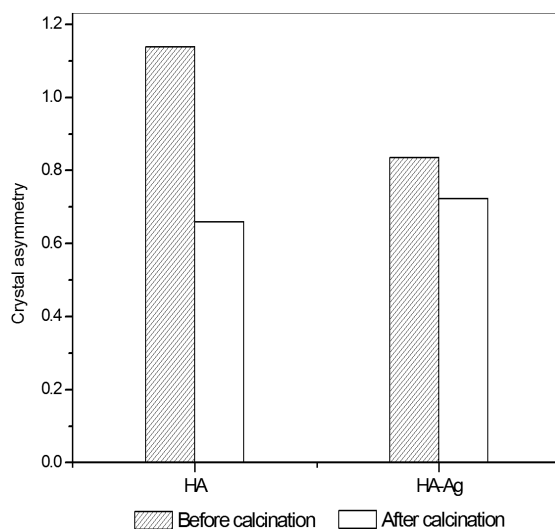


**Figure 8.** Crystal asymmetry calculated from the X-ray diffraction patterns of the samples before and after calcination.

increased, and they were homogeneously distributed on the HA crystals. The agglomerate size increased until 70 hours, when the particle morphology became notably different from the originally observed morphology.

According to the X-ray diffraction patterns of the HA samples and the Rietveld refinement after 1, 24, 48 and 70 h of immersion, a new crystalline phase of Ag<sub>3</sub>PO<sub>4</sub> (ICDD 06-0505) was formed on the original HA crystals (Figure 10), which suggests that the Ag<sup>+</sup> ions reacted with the PO<sub>4</sub><sup>3-</sup> groups on the surface to form the new Ag<sub>3</sub>PO<sub>4</sub> phase. Even within 1 hour of immersion, some Ag<sub>3</sub>PO<sub>4</sub> clusters were observable in the samples.

The changes in the crystal morphology of HA during immersion, which were revealed using transmission electron microscopy, suggest that the Ag<sup>+</sup> ions were not confined only

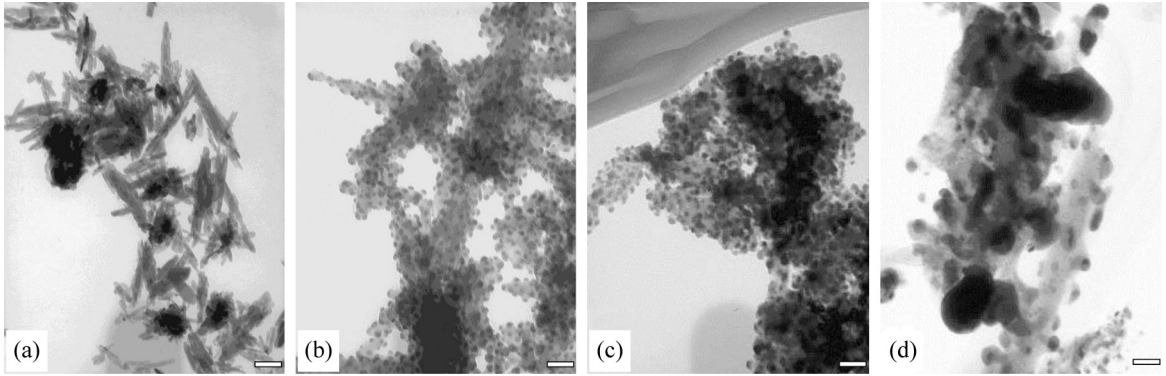


**Figure 9.** TEM images showing the HA crystals, which were covered with electron-dense clusters after immersion in a  $\text{AgNO}_3$  solution for 1 (a), 24 (b), 48 (c) and 70 h (d). Bar = 200 nm.

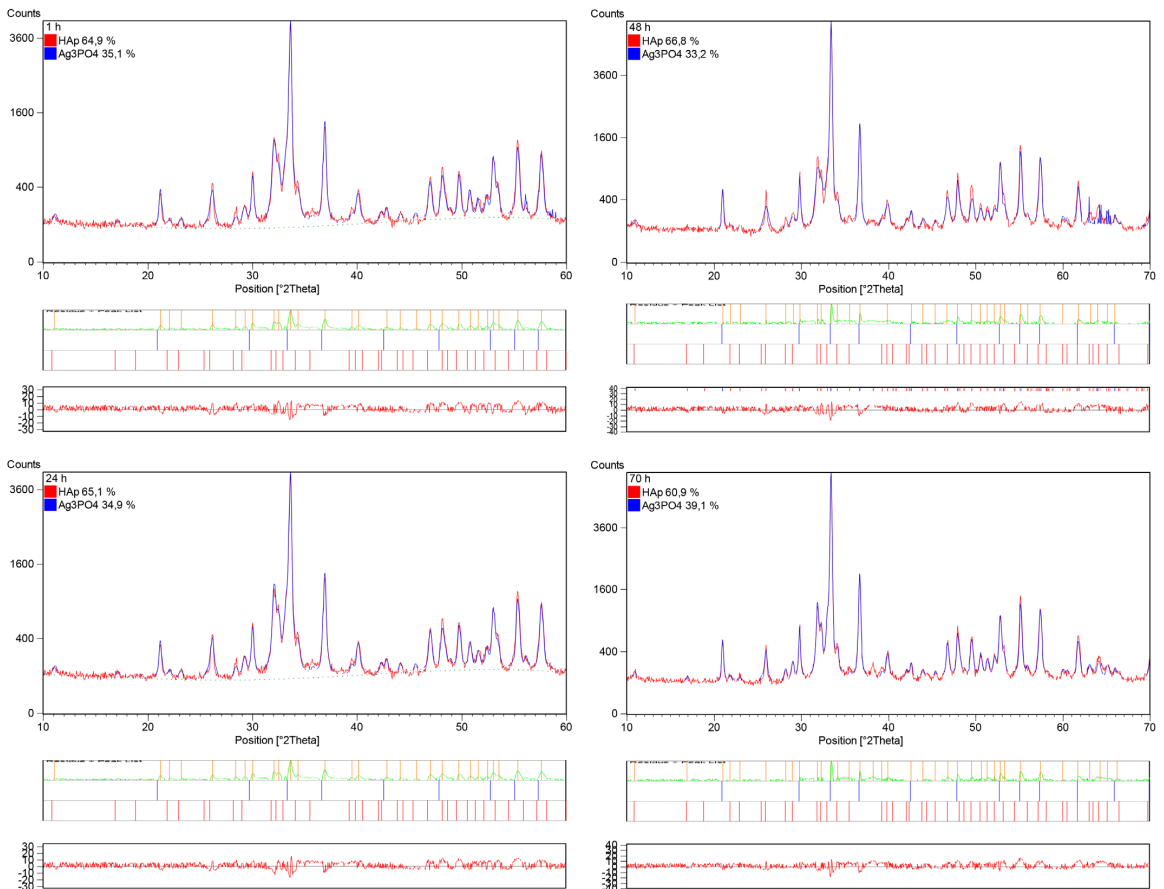


**Figure 10.** X-ray diffraction patterns of the HA samples after immersion for 1, 24, 48 and 70 h in a silver nitrate solution. Hydroxyapatite (HAp) and silver phosphate ( $\text{Ag}_3\text{PO}_4$ ) phases were identified and quantified by Rietveld refinement.

on the surface. To evaluate the possible insertion of  $\text{Ag}^+$  ions into the HA structure as a function of the immersion time, the lattice parameters were calculated from the Rietveld refinement for each immersion time. The results indicated that the immersion for 1 hour was sufficient to remarkably change the  $a$  and  $c$  lattice parameters compared to the original HA (Figure 11). After this time, the values remained almost

constant until 70 h. Therefore, we conclude that  $\text{Ag}^+$  ions can be inserted into the HA lattice either during the synthesis in the presence of these ions or by ionic diffusion from an aqueous solution that contains  $\text{Ag}^+$ , which allows us to propose less complex routes for doping hydroxyapatite implantable devices with  $\text{Ag}^+$  and avoid phase transformation problems at high temperatures.

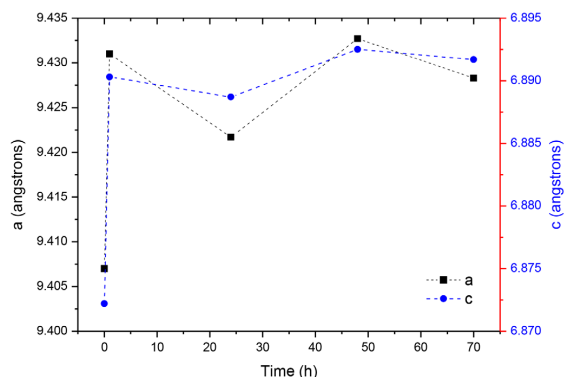


**Figure 11.** Changes in the lattice parameters of the HA after immersion in a silver nitrate solution for 1, 24, 48 and 70 h.

## 4. Conclusion

Despite having different radii, the accommodation of Ag<sup>+</sup> ions in the Ca<sup>2+</sup> sites of the hydroxyapatite lattice can be explained by the models proposed for inserting

monovalent ions such as Na<sup>+</sup>. In this case, because Ag<sup>+</sup> ions are larger than Ca<sup>2+</sup> ions and have different charges, Ag<sup>+</sup> ions are stabilized in the HA structure because of a co-substitution with CO<sub>3</sub><sup>2-</sup> ions in both the A- and B-type sites. This simultaneous insertion of Ag<sup>+</sup> and CO<sub>3</sub><sup>2-</sup> appears to thermally stabilize the HA phase because no phase transformation was observed after calcination. In addition, hydroxyapatite can be doped with Ag<sup>+</sup> ions using two routes: co-precipitation in the presence of these ions or diffusion in preformed hydroxyapatite crystals. This result appears to indicate the possibility of doping HA with Ag<sup>+</sup> using less complex routes at ambient temperature and with prefabricated implants or biomaterials to reduce the production costs of devices with antibiotic action.

## Acknowledgements

The authors acknowledge financial support from by the Brazilian research agencies FAPITEC/SE, FAPERJ, CAPES and CNPq.

## References

- Huh AJ and Kwon YJ. "Nanoantibiotics": a new paradigm for treating infectious diseases using nanomaterials in the antibiotics resistant era. *Journal of Controlled Release*. 2011; 156(2):128-145. <http://dx.doi.org/10.1016/j.jconrel.2011.07.002>. PMID:21763369.
- Marambio-Jones C and Hoek E. A review of the antibacterial effects of silver nanomaterials and potential implications for human health and the environment. *Journal of Nanoparticle Research*. 2010; 12(5):1531-1551. <http://dx.doi.org/10.1007/s11051-010-9900-y>.
- Zhang Y, Yin QS, Zhang Y, Xia H, Ai FZ, Jiao YP, et al. Determination of antibacterial properties and cytocompatibility of silver-loaded coral hydroxyapatite. *Journal of Materials Science. Materials in Medicine*. 2010; 21(8):2453-2462. <http://dx.doi.org/10.1007/s10856-010-4101-x>. PMID:20526656.
- Zhang Y, Yin QS, Zhao HF, Li J, Wei YT, Cui FZ, et al. Antibacterial and biological properties of silver-loaded coralline hydroxyapatite. *Frontiers of Materials Science in China*. 2010; 4(4):359-365. <http://dx.doi.org/10.1007/s11706-010-0112-2>.
- Rameshbabu N, Sampath Kumar TS, Prabhakar TG, Sastry VS, Murty KVGK and Prasad Rao K. Antibacterial nanosized silver substituted hydroxyapatite: synthesis and characterization. *Journal of Biomedical Materials Research. Part A*. 2007; 80(3):581-591. <http://dx.doi.org/10.1002/jbm.a.30958>. PMID:17031822.
- Badroul L, Sadel A, Zahir M, Kimakh L and El Hajbi A. Synthesis and physical and chemical characterization of Ca10Ag10-x(PO4)6(OH)2-xx apatites. *Annales de Chimie--Science des Materiaux*. 1998; 23(1-2):61-64. [http://dx.doi.org/10.1016/S0151-9107\(98\)80012-3](http://dx.doi.org/10.1016/S0151-9107(98)80012-3).
- Sygnatowicz M, Keyshar K and Tiwari A. Antimicrobial properties of silver-doped hydroxyapatite nano-powders and thin films. *Journal of the Minerals Metals & Materials Society*. 2010; 62(7):65-70. <http://dx.doi.org/10.1007/s11837-010-0111-x>.
- Nath S, Kalmodia S and Basu B. Densification, phase stability and in vitro biocompatibility property of hydroxyapatite-10 wt% silver composites. *Journal of Materials Science. Materials in Medicine*. 2010; 21(4):1273-1287. <http://dx.doi.org/10.1007/s10856-009-3939-2>. PMID:19967432.
- Singh B, Dubey AK, Kumar S, Saha N, Basu B and Gupta R. In vitro biocompatibility and antimicrobial activity of wet chemically prepared Ca10-xAgx(PO4)6(OH)2 (0.0 ≤ x ≤ 0.5) hydroxyapatites. *Materials Science and Engineering C*. 2011; 31(7):1320-1329. <http://dx.doi.org/10.1016/j.msec.2011.04.015>.
- Silva LM, Menezes DS, Almeida LE, Anselme K, Dentzer J and Santos EA. The role of the counter-ions present in syntheses on the thermal stabilization of strontium and/or calcium apatites. *Materials Science and Engineering B*. 2015; 199:77-86. <http://dx.doi.org/10.1016/j.mseb.2015.05.003>.
- Moreira MP. *Produção de hidroxiapatita enriquecida com metais biofuncionais para aplicação em engenharia tecidual*. [Dissertation]. Sergipe: Universidade Federal de Sergipe; 2011.
- Moreira MP, Aragão VTS, Soares GA and Santos EA. Simultaneous insertion of Mg<sup>2+</sup>, Sr<sup>2+</sup> and Mn<sup>2+</sup> ions into hydroxyapatite structure. *Key Engineering Materials*. 2012; 493-494:20-26. <http://dx.doi.org/10.4028/www.scientific.net/KEM.493-494.20>.
- Aina V, Lusvardi G, Annaz B, Gibson IR, Imrie FE, Malavasi G, et al. Magnesium- and strontium-co-substituted hydroxyapatite: the effects of doped-ions on the structure and chemico-physical properties. *Journal of Materials Science. Materials in Medicine*. 2012; 23(12):2867-2879. <http://dx.doi.org/10.1007/s10856-012-4767-3>. PMID:23053798.
- Kumar GS, Thamizhavel A, Yokogawa Y, Kalkura SN and Girija EK. Synthesis, characterization and in-vitro studies of zinc and carbonate co-substituted nano-hydroxyapatite for biomedical applications. *Materials Chemistry and Physics*. 2012; 134(2-3):1127-1135. <http://dx.doi.org/10.1016/j.matchemphys.2012.04.005>.
- Mostafa NY, Hassan HM and Abd Elkader OH. Preparation and characterization of Na<sup>+</sup>, SiO<sub>4</sub><sup>4-</sup>, and CO<sub>3</sub><sup>2-</sup> Co-substituted hydroxyapatite. *Journal of the American Ceramic Society*. 2011; 94(5):1584-1590. <http://dx.doi.org/10.1111/j.1551-2916.2010.04282.x>.
- Stokes AR, Wilson AJC and Bragg WL. A method of calculating the integral breadths of Debye-Scherrer lines. *Mathematical Proceedings of the Cambridge Philosophical Society*. 1942; 38(03):313-322. <http://dx.doi.org/10.1017/S0305004100021988>.

17. Yao F, LeGeros JP and LeGeros RZ. Simultaneous incorporation of carbonate and fluoride in synthetic apatites: Effect on crystallographic and physico-chemical properties. *Acta Biomaterialia*. 2009; 5(6):2169-2177. <http://dx.doi.org/10.1016/j.actbio.2009.02.007>. PMID:19269268.
18. Boanini E, Gazzano M and Bigi A. Ionic substitutions in calcium phosphates synthesized at low temperature. *Acta Biomaterialia*. 2010; 6(6):1882-1894. <http://dx.doi.org/10.1016/j.actbio.2009.12.041>. PMID:20040384.
19. Fernández E, Gil FJ, Ginebra MP, Driessens FCM, Planell JA and Best SM. Calcium phosphate bone cements for clinical applications. Part I: solution chemistry. *Journal of Materials Science. Materials in Medicine*. 1999; 10(3):169-176. <http://dx.doi.org/10.1023/A:1008937507714>. PMID:15348165.
20. Elliot JC. *Structure and chemistry of the apatites and other calcium orthophosphates*. London: Elsevier; 1994.
21. Vignoles C. *Contribution a' l'étude de l'influence des ions alcalins sur la carbonatation dans les sites de type B des apatites phospho-calcique*. [Thesis]. Toulouse: Université Paul Sabatier; 1973.
22. Wilson RM, Elliott JC, Dowker SEP and Smith RI. Rietveld structure refinement of precipitated carbonate apatite using neutron diffraction data. *Biomaterials*. 2004; 25(11):2205-2213. <http://dx.doi.org/10.1016/j.biomaterials.2003.08.057>. PMID:14741636.
23. Fleet ME and Liu X. Coupled substitution of type A and B carbonate in sodium-bearing apatite. *Biomaterials*. 2007; 28(6):916-926. <http://dx.doi.org/10.1016/j.biomaterials.2006.11.003>. PMID:17123599.
24. Silva LM. *Estabilização estrutural de apatitas de cálcio e/ou estrôncio via co-substituições iônicas*. [Dissertação]. Sergipe: Universidade Federal de Sergipe; 2014.
25. Dubnika A and Zalite V. Preparation and characterization of porous Ag doped hydroxyapatite bioceramic scaffolds. *Ceramics International*. 2014; 40(7):9923-9930. <http://dx.doi.org/10.1016/j.ceramint.2014.02.088>.
26. Uskoković V and Uskoković DP. Nanosized hydroxyapatite and other calcium phosphates: chemistry of formation and application as drug and gene delivery agents. *Journal of Biomedical Material Research Part B*. 2011; 96(1):152-191. <http://dx.doi.org/10.1002/jbm.b.31746>. PMID:21061364.
27. Hwang KS, Hwangbo S and Kim JT. Silver-doped calcium phosphate nanopowders prepared by electrostatic spraying. *Journal of Nanoparticle Research*. 2008; 10(8):1337-1341. <http://dx.doi.org/10.1007/s11051-008-9404-1>.